Sensors and Materials, Vol. 36, No. 2 (2024) 779–794
MYU Tokyo

S & M 3561

Development of Impedance Electrode Detection Strips for Quantitative Detection of Human Chorionic Gonadotropin

Wei-Chien Weng,[1] Yu-Lin Wu,[1] Hsin-Yu Chen,[1] and Yu-Cheng Lin[1,2*]

[1]Department of Engineering Science, National Cheng Kung University,
No. 1, University Road, Tainan City 70101, Taiwan
[2]Institute of Innovative Semiconductor Manufacturing, National Sun Yat-sen University,
No. 70, Lien-hai Road, Kaohsiung City 804201, Taiwan

(Received September 22, 2023; accepted February 13, 2024)

Keywords: impedance electrode chip, electrical measurement, rapid test, hCG concentration detection, lateral flow immunochromatography, gold nanoparticles, phase transformation

In this study, an impedance electrode chip that we developed was used for the detection of human chorionic gonadotropin (hCG) sandwich immunoreactivity, as well as gold nanoparticle (AuNP)-conjugated antibodies as labels to facilitate detection. The immune response of the tested specimen and quantitative impedance measurement analysis results were used for identification. An LCR meter, which is a type of electronic test equipment used to measure the inductance (L), capacitance (C), and resistance (R) of an electronic component, was used to detect the electrical signal of the impedance electrode chip, and the changes in immune response were analyzed through impedance value changes to establish the electrical measurement data of hCG. To avoid signal measurement problems caused by poor bonding between the nitrocellulose (NC) membrane and the detection electrode, the NC membrane was fixed directly onto the surface of the detection electrode by a polymer solution phase conversion method, and quantitative impedance signals at different hCG concentrations were successfully measured. The results showed that using this method successfully broke through the traditional naked-eye identification concentration limit of 25 mIU/mL, reaching a lower concentration of 6.25 mIU/mL, and the coefficient of determination between the impedance value signal and the hCG concentration reached 0.9899, which means that the self-made electrode chip can quantitatively detect and analyze the hCG concentration.

1. Introduction

With the advancement of science and technology, people's living standards have also been improved. In the past, the methods of detecting disease problems often frightened patients, leading to the rapid exacerbation of the disease. The development and popularization of rapid screening reagents have resulted in many more choices for disease screening. Rapid tests are being applied in areas such as pregnancy, cancer, diabetes, influenza, and animal diseases.

*Corresponding author: e-mail: yuclin@mail.ncku.edu.tw
https://doi.org/10.18494/SAM4799

ISSN 0914-4935
https://myukk.org/

Furthermore, with the appearance of COVID-19, which has affected the world in recent years, it has been shown that the application of rapid tests can quickly and effectively control the progress of global epidemics. In this study, an electrode detection technology for rapid tests is developed. By utilizing a new nitrocellulose (NC) membrane combined with electrodes, both designed and fabricated by us, as well as the characteristics of gold nanoparticles, we achieved a transformation of rapid tests from the traditional qualitative detection to quantitative detection.

Rapid tests are also called lateral flow chromatography immune reaction detection tests. Their principle includes physical and chemical methods. The physical aspect is to use the pore size on a sample pad to filter interference in the sample to be tested. As it passes through the sample pad, the sample combines with the gold nanoparticles bonded with the secondary antibody on the conjugate pad and continues to flow in the direction of the wicking paper owing to the capillary force generated by the NC membrane.[1]

The conjugation of antigen and antibody mainly occurs at the interaction site between the antigen and the antibody. The site where the antigen is recognized by the antibody is called the epitope, which usually consists of 4 to 5 amino acids and 4 to 5 monosaccharides. The binding forces between antigens and antibodies include Coulomb electrostatic force, hydrogen bonds, hydrophobic force, and Van der Waals force, but there is also another electrostatic repulsive force. All forces form a total bonding force. Because the binding between the antigen and the antibody is not a covalent bond, changes in the environment, such as changes in pH, temperature, and ionic strength, may cause the antigen and antibody to separate from each other,[2, 3] altering the bonding force between the antigen and the antibody and thereby causing different color effects on the test line.

In this study, human chorionic gonadotropin (hCG) is used to produce rapid tests as experimental samples. hCG is a glycoprotein hormone with a molecular mass of 36.7 kDa.[4] It is composed of two different subunits, α and β. The α subunit is combined with other glycoprotein hormones secreted by the pituitary gland, such as luteinizing hormone (LH) and follicle-stimulating hormone (FSH), and is almost identical to the α subunit of thyroid-stimulating hormone (TSH),[5] but the largest difference lies in the different structures of the β subunits.[6] Regardless of age, the pituitary glands of all men and women can produce gonadotropins similar to hCG, such as LH and other types of hormone.[7,8] In 2018, Casarini *et al.* proposed a study on the relationship between hCG and malignant tumors.[8] hCG is secreted by the placenta during pregnancy, and the gonadotropin secreted by the placenta is called chorionic gonadotropin; however, in the urine of pregnant women, the chorionic gonadotropin is called hCG. Because hCG is similar to LH, hCG is also used clinically to induce ovulation and produce testosterone. Women who are in the early stage of pregnancy are the main source of hCG. Some institutions even collect the urine of pregnant women to extract hCG for fertility treatment.[9] hCG can also be used as a tumor marker. The secretion of its β subunit can be observed in some cancers, including seminoma, choriocarcinoma, germ cell tumor, vesicular fetal mass, teratoma, and islet cell tumor.[10,11]

When a urine specimen with hCG antigen is dropped onto the sample pad of the immune rapid test, the specimen flows forward to the conjugate pad. This conjugate pad contains freeze-dried high-dose hCG second antibody–colloidal gold conjugate (hCG–GC). The hCG antigen in

the urine undergoes a conjugation reaction with hCG-GC in the conjugate pad. This reaction is a specific immune reaction, so non-hCG antigen specimens will not conjugate with this antibody. The NC membrane continues to drive the urine to the test line and combines with the hCG primary antibody presprayed onto the test line. This reaction is also a specific immune reaction. The position of the test line also appears purplish red (the color of the gold nanoparticles) due to the aggregation of the gold nanoparticles. This is the immunochromatic method of rapid testing.[12] The primary antibody is also called coating Ab because it is sprayed on the T line, and the secondary antibody is bonded to gold nanoparticles and called detection Ab.

In realizing rapid tests, the porosity of the NC membrane is particularly important. During production, the polymer material is converted from the liquid phase to the solid phase by the phase inversion method.[13,14] The casting solution prepared from three components, polymer, volatile solvent, and nonvolatile nonsolvent, is a homogeneous solution at a certain fixed temperature. The solvent gradually evaporates during the constant temperature process. The volatilization of the solvent causes the phase separation of the solution from a homogeneous phase, resulting in a solution with two phases, namely, a polymer-poor phase and a polymer-rich phase. The polymer-rich phase represents the phase state with high polymer concentration, while the polymer-poor phase represents the phase state with low polymer concentration. After the solvent completely evaporates, the solubility of the polymer decreases, and a porous film structure is formed because of the phase separation behavior. The polymer-rich phase solidifies to form the main body of the film, while the polymer-poor phase forms a continuous hole structure. Phase inversion methods mainly include thermally induced phase separation,[15–19] solvent evaporation,[20,21] immersion precipitation,[22,23] and vapor-induced phase separation.[24–28]

During film formation, the study of the three polymer–solvent–nonsolvent components is the basis for exploring the film formation mechanism.[29–33] Among them, the ternary phase diagram of the Flory–Huggins theory is used to describe the thermodynamic behavior of the polymer solution, and the gravitational parameters between the components are used to obtain the relationship of the Gibbs free energy of mixing (ΔG_m) versus temperature and composition.[34–37] The film formation process consists of a homogeneous polymer solution (V area). Depending on the solvent and nonsolvent proportions, NC membranes can correspond to (I, VI) dense structures, (II) sponge structures, (III) bicontinuous or lacy structures, and (IV) nodules. Therefore, the possible film structure type can be preliminarily determined on the basis of the system components using the thermodynamic phase diagram.[38,39]

The detection mechanism used in this study is wet impedance measurement, which considers the aggregation of gold nanoparticles after the antibody–antigen reaction on the surface of the rapid tester to conduct electrical signals. On the basis of the principle that the number of gold nanoparticles affects the signal conduction ability, resistance can be used to detect changes in the concentration of the sample to be tested.[40–45]

2. Materials and Methods

This paper is divided into four parts to discuss the construction of the entire system: the preparation of the NC membrane for rapid tests, the design of impedance electrodes, the combination of the NC membrane and electrodes, and signal measurement.

2.1 Porous membrane preparation

First, the raw materials for the preparation of the NC membrane include NC polymer and 30% isopropyl alcohol, methyl acetate (MA) and acetone as solvents, and isopropyl alcohol (IPA), glycerin, and deionized (DI) water as nonsolvents in coatings. NC polymer (9.2 wt%) is prepared by dissolving in 5.2 wt% MA and 52.8 wt% acetone. When the NC polymer is completely dissolved in the MA and acetone solution, 22 wt% IPA, 5 wt% glycerol additive, and 5.6 wt% water are added as pore formers. The NC film is prepared by the dry-phase inversion method. The film is fixed on the surface of the electrode wafer and kept in a certain relative humidity environment. Phase inversion is induced through the absorption of water vapor and the evaporation of acetone for 1 h. In the final step, the NC film is dried in a vacuum oven at 30 °C for 2 h, and excess nonsolvent is removed from the polymer. Finally, a scanning electron microscopy (SEM) system is used to observe the cross section, surface, thickness, and pore size of the film, and the porosity calculation method is used to conduct porosity research.

The porosity (ε) is calculated as

$$\varepsilon = \frac{V_A - V_E}{V_A} \times 100\% , \tag{1}$$

where V_A, which is the apparent volume of the NC membrane, is calculated from the thickness and surface area of the membrane. V_E, which is the actual volume of the NC membrane, is determined from the density of the polymer (1.23 g/cm^3) and the weight of the NC membrane.

2.2 Design of resistive electrode

Among the resistive electrode materials, common ones include silver paste, indium tin oxide (ITO), and gold chromium. Among them, silver paste is a commonly used electrode material for detection by the rapid test. It is a conductive paste composed of silver powder, resin, solvent and adhesive. It achieves high conductivity through the silver powder in the composition and has low resistance and high adhesion properties. It can be used to form stable and precise circuits on polyethylene terephthalate (PET) printed substrates. It also has good printing properties and high reliability, and can improve the conductivity and stability of printed electrodes. Silver paste printed electrodes have the advantages of good electrode position consistency, which can reduce experimental errors, and small impedance to avoid affecting concentration discrimination. Therefore, silver paste printed electrodes are selected as detection electrodes.

The computer-aided design (CAD) software AutoCAD® 2018 (Autodesk, USA) was used to design the electrodes. The purpose of the pattern design on an electrode is to enable the reaction

area in the middle of the electrode to effectively complete the input and reception of signals, and to consider the change in the impedance of its current transmission during conduction. Therefore, the pattern gradually changes from a large area (signal connection end) and narrows down to a small area. The microelectrode tip helps reduce the impedance generated by the electrode itself, and the signal connection end can be connected to external equipment. To provide the space required for lateral flow chromatography rapid test manufacturing, the plastic substrate is drawn to an area of 76 × 26 mm^2 to ensure the integration space for the absorbent, sample, and conjugate pads. The detection electrode pattern design is shown in Fig. 1(a). The signal measurement part is designed to be 2000 μm wide, as shown in Fig. 1(b), and the space between parallel electrodes is 300 μm, which is the detection area used for impedance measurement, as shown in Fig. 1(c).

2.3 Combination of impedance measurement electrode and lateral flow immunochromatography rapid test

According to previous research, the gap between commercially available NC membranes and electrodes can easily cause instability in electrical impedance signal measurement. To solve the compatibility problem between the two, our homemade NC membrane is coated on the interface of the detection chip. The NC membrane is prepared using NC, acetone, MA, IPA, glycerol, and

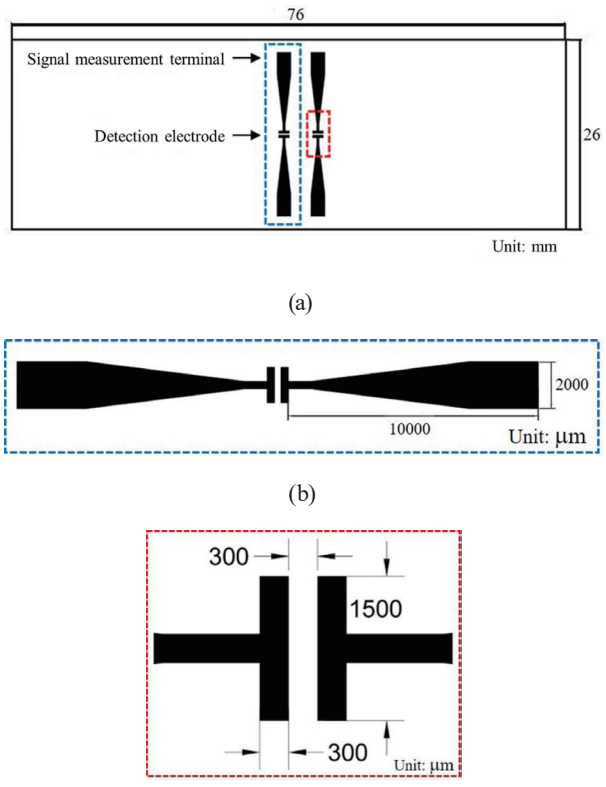

Fig. 1. (Color online) Schematic of designed resistive electrode dimensions: (a) detection electrode pattern design, (b) signal measurement design, and (c) detection area electrode size.

DI water. The dry-phase inversion method is used to convert NC from liquid to solid, and then the resulting NC membrane is combined with the glass substrate by the three-component casting solution with a homogeneous solution of polymers, volatile solvents, and nonvolatile nonsolvents at a certain fixed temperature. After the solvent is gradually completely evaporated in a constant-temperature program, the solubility of the polymer decreases, and a porous film structure is formed owing to the phase separation behavior. Among them, acetone and MA are used as volatile solvents, and the nonvolatile nonsolvents are IPA and glycerol. The volatilization rate and phase separation behavior of the solvent and nonsolvent are the main control variables. We use a vacuum at a constant temperature to dry the completed NC membrane. When water is in a high-vacuum environment and is below the triple point, it can only exist in the solid and gaseous states at any temperature. Therefore, we exploit this characteristic by heating the sample under high vacuum. At this time, the water in the sample will directly sublimate into a gas, thereby achieving the purpose of drying.

The lateral flow chromatography structure manufacturing process is divided into four major components. The first component is the sample pad. The sample pad is the first component to contact the solution to be tested. Therefore, the sample pad maintains functions such as filtration and flow rate control. The second component is a colloidal gold film (gold nanoparticle–secondary antibody film), which is sprayed on glass fiber paper with gold nanoparticles bonded with hCG secondary antibody (hCG-GC). The antigen in the solution to be tested will be captured by the secondary antibody on the gold nanoparticles. Therefore, the buffer solution on the gold nanoparticle–secondary antibody membrane is a key factor in determining whether the antigen can be stably captured. The third component is the NC membrane. The NC membrane is sprayed with a control line (C line) and a test line (T line). The C line comprises the mouse antibody and the T line comprises the hCG primary antibody. The fourth component is the absorbent pad, whose capillary force is the key factor in generating flow throughout the entire lateral flow chromatography test paper. The schematic diagram of the combination of the lateral flow immunochromatography rapid test and impedance measurement electrode is shown in Fig. 2, which shows the sample pad, conjugate pad, NC membrane, detection electrode, and wicking paper. Figure 3 shows the actual physical diagram produced in this study.

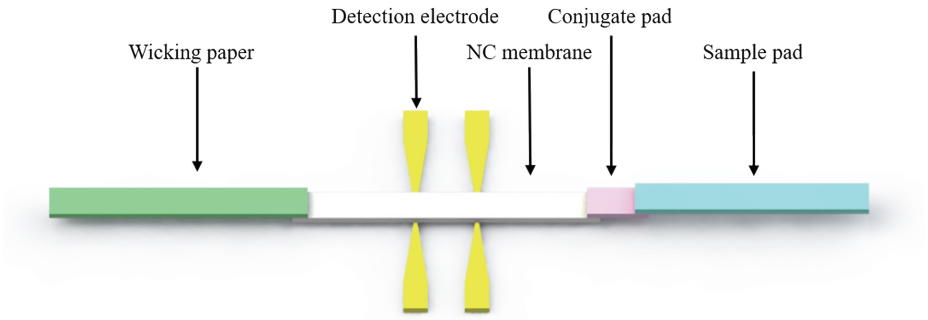

Fig. 2. (Color online) Schematic drawing of impedance detection electrode chip.

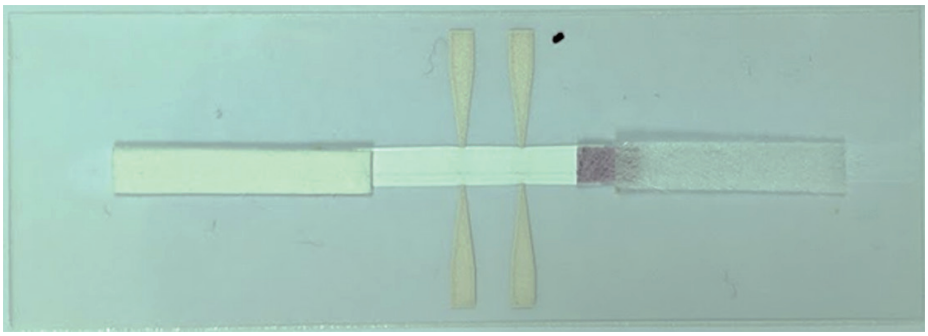

Fig. 3. (Color online) Physical diagram of impedance measurement electrode.

2.4 Measurement of electrical signals

This discussion is divided into two parts. The first part is a discussion of our homemade NC membrane and its performance. By directly phase-converting the NC membrane and fixing it on the surface of the detection electrode, the electrical impedance caused by the gap between the NC membrane and the detection electrode chip can be avoided. An unstable state of signal measurement occurs and the compatibility problem between the two is solved. In the second part, the use of the ELISA sandwich immune method as the basis of the analysis structure is discussed. The immune reaction results on the reagent are electrically measured for different concentrations of hCG, and an impedance immunoassay detection platform is established. Using the principle of lateral flow chromatography, antibody-conjugated gold nanoparticles are immobilized on the glass fiber membrane, and the test sample is continuously transported to the detection area, and the response to the detection sample is seen in the detection area. hCG antigen contents are differentiated as they combine with gold nanoparticles with corresponding contents on the test line, indicating differences in electrical size and achieving quantitative measurement and the analysis of hCG. The immune impedance analysis is shown in Fig. 4.

Finally, after the sample containing hCG flows from the sample pad to the NC membrane, the gold nanoparticles will appear between the electrodes, and the impedance of the gold nanoparticles will be measured through the LCR meter.

3. Results and Discussion

The porosity and thickness of the NC membrane are very important during production. The porosity of the pores of the NC membrane can be controlled by controlling the humidity, and the thickness condition also controls the lateral flow chromatography and how well it combines with electrodes. For the data detection part, we used hCG as the detection sample and a self-designed electrode chip to measure the concentrations of hCG-Ab and hCG, and tested the conditions of hCG at different detection frequencies.

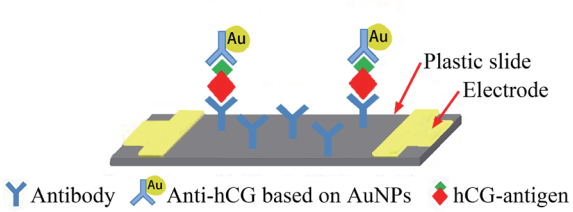

Fig. 4. (Color online) Schematic diagram of immune impedance analysis.

3.1 Humidity control of NC membrane process

The NC membrane manufacturing process in this paper uses the polymer phase conversion membrane mechanism to convert the polymer NC solution into a continuous hole structure of the film, where the principle of lateral flow chromatography is used to drive the gold nanoparticles to the film detection area to bond with primary antibodies and subsequent impedance measurements are taken. In the phase transition of polymer solutions, humidity is the main factor that controls the pore structure. Therefore, porosity is discussed under the condition of phase transition with different values of relative humidity (RH). The experimental humidity ranges from 65 to 90% RH, and three repeated experiments are conducted at intervals of 5% RH. The RH and porosity analysis chart is shown in Fig. 5.

Experimental results show that in phase conversion, 75–80% RH results in higher porosity. The average porosity at 75% RH is 57.63%, whereas the porosity at 80% RH is 53.77%. If the porosity is higher, the NC membrane will have a higher ability to carry gold nanoparticles for lateral flow chromatography, so that the concentration of the antigen to be detected has higher discrimination. According to the research data on porosity, 80–90% RH also leads to higher porosity, so a SEM system is used to study the surface structure of the NC membrane, as shown in Fig. 6.

In the SEM images of the surface structure of the NC membrane, the pore sizes of the surface structure at 75% RH and 90% RH are compared, and the gold nanoparticles used in this experiment are found to have a particle size of 40 nm, which is suitable for NC with a molecular size of about 10 μm. The size of the membrane pores matches the pore size obtained under the phase conversion condition of 75% RH. Under the phase conversion condition of 90% RH, the surface pores are of different sizes, and some surfaces have no pores, which will cause the primary antibody coating in the T-line detection area to be ineffective and gold nanoparticles cannot smoothly enter the NC membrane pores. Consequently, the conjugate of antigen–Au nanoparticles–secondary antibodies cannot be captured in the detection area, resulting in failure of the test. Therefore, under the phase inversion condition of 75–80% RH, the pore size is consistent with the particle size of the gold nanoparticles used and the surface pores are relatively uniform. Hence, this humidity range is selected as the optimal phase inversion condition.

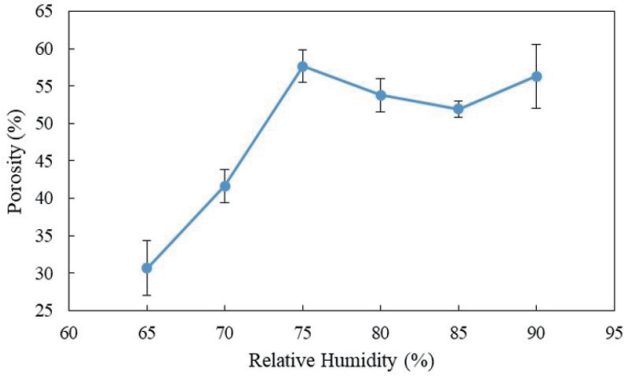

Fig. 5. (Color online) Phase-conversion relative humidity and porosity.

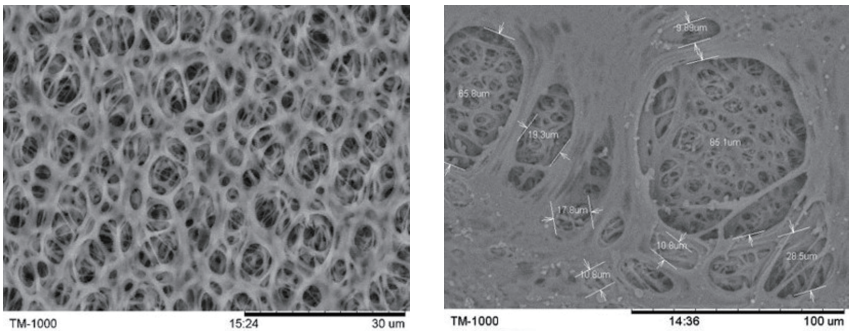

(a) (b)

Fig. 6. SEM images of surface structure of NC membrane under phase conversion conditions of (a) 75% RH and (b) 90% RH.

3.2 Structure and thickness of NC membrane

In the NC membrane structure, in addition to the surface structure, the overall structure is also very important. If the overall structure is poor, the porosity will be very low, and the antigen cannot be successfully transferred to the detection area of the NC membrane. Therefore, a SEM system is used to study the cross-sectional structure and thickness of the NC membrane, as shown in Fig. 7.

In the cross-sectional structure of the NC membrane, under observation with a SEM system, the NC membrane exhibits a dense continuous hole structure with a thickness of approximately 68 μm and has a less blocky structure that blocks gold nanoparticles. The continuous hole structure facilitates the delivery of the antigen, secondary antibodies, and gold nanoparticles to the T-line detection area of the NC membrane. The primary antibody is coated on the T line to capture the antigen, and the antigen connects the secondary antibody and gold nanoparticles. If the gold nanoparticles are blocked by the discontinuous hole structure and cannot flow smoothly to the detection area, the backend of the NC membrane is damaged. In impedance measurement, for the same concentration of antigen, different amounts of gold nanoparticles are present,

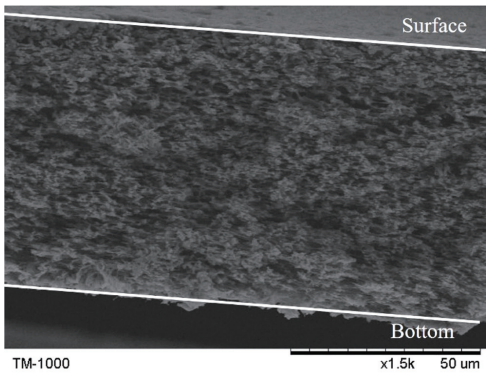

Fig. 7. Cross-sectional structure of NC membrane.

resulting in impedance differences. In this study, we successfully produced an NC membrane with a dense and continuous hole structure in its cross section, which helps the backend impedance measurement to discriminate various concentrations.

3.3 hCG-Ab concentration test

In the sandwich immune reaction detection experiment, the detection base hCG-Ab parameters are fixed, so in this experiment, three different concentrations of hCG-Ab (5, 2.5, and 1.25 mg/mL) are used to detect three concentrations of the hCG test antigen (37.5, 25, and 12.5 mIU/mL) with a gold nanoparticle-secondary antibody membrane (hCG-GC) concentration of 8 μg/mL for immune detection. The frequency is set to 1000 Hz. Each concentration of hCG-Ab corresponds to the impedance of each hCG concentration. The analysis results are shown in Fig. 8.

The results in Fig. 8 show that hCG-Ab with a concentration of 1.25 mg/mL corresponds to three different concentrations of hCG antigen. Compared with hCG-Ab at other concentrations, the standard deviation is larger, which means that the antibody parameters measured using hCG-Ab at a concentration of 1.25 mg/mL are less stable and its concentration discrimination is lower. The possible reason is that the concentration of hCG-Ab is very low, which prevents the hCG antigen from effectively conjugating with hCG-Ab, resulting in a relatively small amount of antibody-conjugated gold nanoparticles in the sandwich immune reaction, leading to increased impedance and error. In the study of hCG-Ab at 5 mg/mL, its impedance discrimination was smaller than that of hCG-Ab at 2.5 mg/mL. Therefore, in the experiments, we used hCG-Ab with an experimental concentration of 2.5 mg/mL as the subsequent experimental standard.

3.4 Relationship between hCG impedance and frequency

To explore how to measure the impedance differences of hCG antigen at different concentrations at different frequencies, an LCR meter is used for detection. In this experiment,

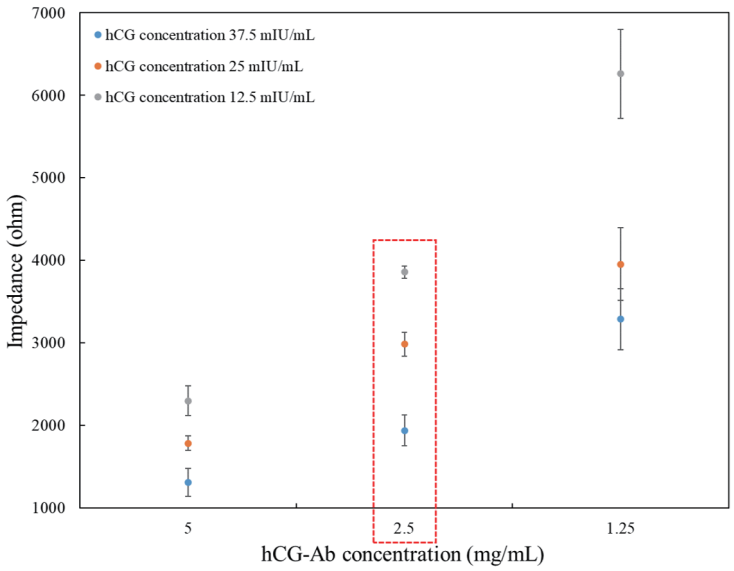

Fig. 8. (Color online) Impedance analysis diagram of different concentrations of hCG-Ab corresponding to each concentration of hCG.

we discuss the impedance electrical detection results of the sandwich immune reaction of hCG antigen at various concentrations in the frequency range of 100–1200 Hz. The impedance detection electrode chip is used to conduct the impedance sweep analysis of the hCG antigen at 12.5, 25, 37.5, and 50 mIU/mL. The detection results are shown in Fig. 9.

When detecting different concentrations of hCG antigen, the impedance difference between concentrations is the largest at the low frequency of 100 Hz, but the standard deviation is very large, resulting in the low concentration discrimination and stability of each concentration at low frequencies. At 1100 Hz, the impedance difference between the concentrations is small, which also means that the concentration discrimination is low. Particularly at the higher concentrations of the antigen to be tested, 50 and 37.5 mIU/mL, the concentration discrimination is low. Considering that the standard deviation has overlapped the impedance values of different antigen concentrations, the frequency of 1100 Hz is not used. Compared with the low frequency of 100 Hz and the high frequency of 1200 Hz, when the frequency is 1000 Hz, the standard deviation will not be so large as to cause the misjudgment of each concentration, and there is also a clear concentration discrimination. It can be concluded that under the impedance detection electrode chip and detection mechanism, using 1000 Hz for the sandwich immune electrical impedance detection of the hCG antigen and taking into account the two factors of concentration discrimination and standard deviation, the concentration discrimination is high and the standard deviation is relatively small, so all the subsequent experiments were measured using the sandwich immune electrical impedance at a frequency of 1000 Hz.

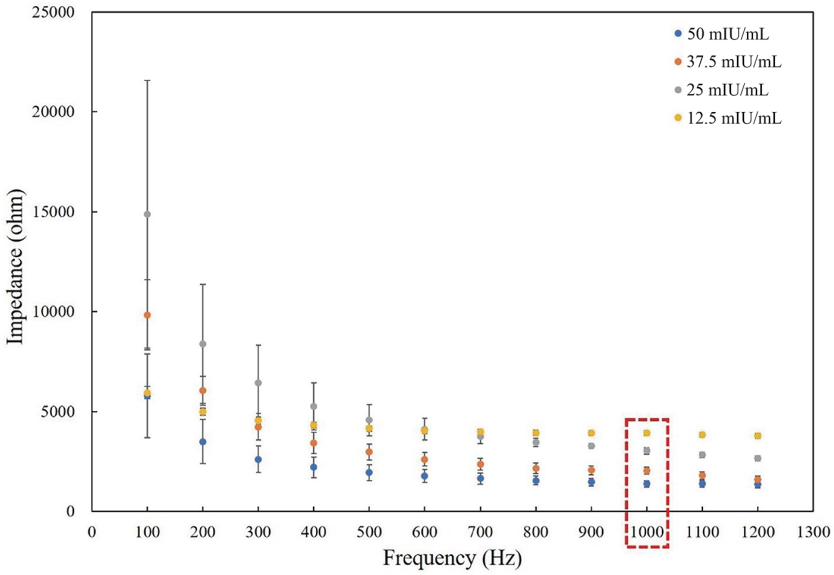

Fig. 9. (Color online) Frequency of sandwich immunoreaction and impedance of hCG antigen.

3.5 hCG detection impedance analysis

The aim of this study is to use electrical impedance to determine the hCG antigen concentration. It is expected that the impedance values at different hCG antigen concentrations will exhibit a clear concentration discrimination. Therefore, the impedance detection electrode chip is used to detect the antigen concentrations of 0, 6.25, 12.5, 25, 37.5, 50, and 100 mIU/mL for impedance measurement and analysis. The measured impedance corresponds to the antigen concentration for impedance trend analysis, as shown in Fig. 10. Each concentration can be discriminated, and the antigen concentration in the sample can be determined by detecting the impedance. Figure 11 shows the color development status of the actual detection using the impedance detection electrode chip. From left to right, the antigen concentrations are 6.25, 12.5, 25, 37.5, and 50 mIU/mL. It can be seen from this figure that the antigen concentration in the specimen cannot be accurately determined by the color depth. Errors and misjudgments are prone to occur, which further highlights the importance of impedance analysis. The threshold of 25 mIU/mL is selected, and concentrations close to the threshold are selected for further calibration line analysis. The linear analysis results are shown in Fig. 12. The antigen concentration in the sample is 6.25–100 mIU/mL and the corresponding impedance range is 1300–4700 ohm. The determination coefficient R^2 (coefficient of determination) of the calibration line detection is 0.9899. The larger the coefficient of determination, the smaller the deviation of the measured impedance points of each concentration from the trend line, and it is easier and more accurate to determine the corresponding concentration of the measured impedance based on the trend curve. The slope of the trend curve is 73.946. The larger the slope of the trend curve, the more obvious the trend of the impedance change corresponding to different concentrations and the greater the discrimination and sensitivity. It can be seen from

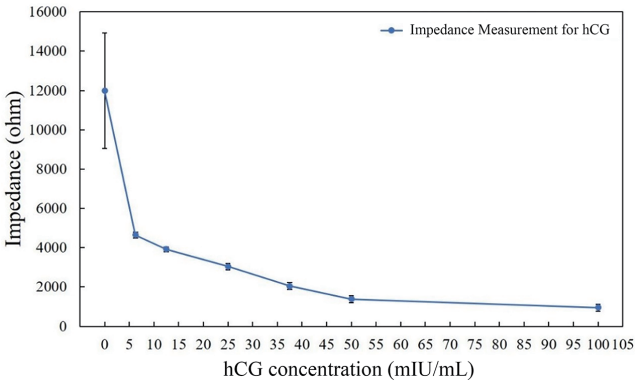

Fig. 10. (Color online) Impedance analysis diagram of hCG antigen.

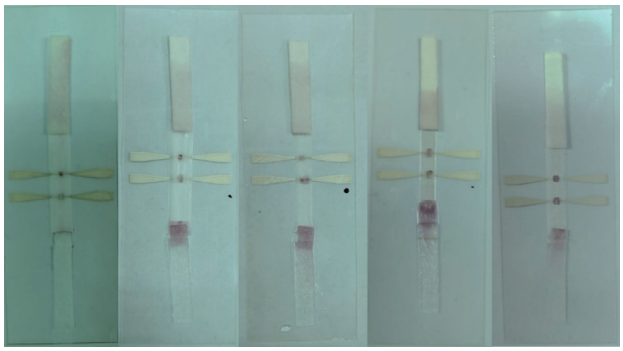

Fig. 11. (Color online) Actual measurement diagram of impedance detection electrode chip.

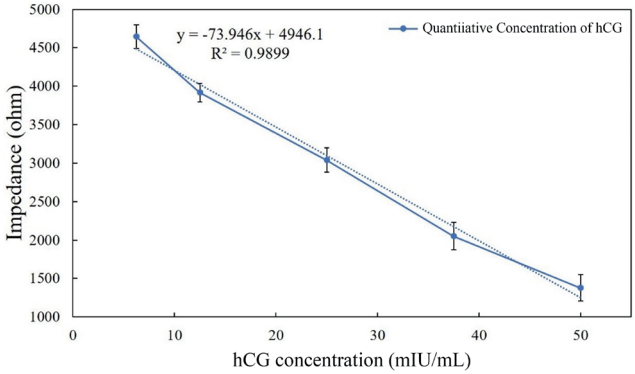

Fig. 12. (Color online) Linear analysis chart of calibration curve of hCG antigen.

the detection line that the impedance detection electrode chip studied has good sensitivity and concentration discrimination. It can determine the antigen concentration contained in the sample through the impedance, solving the shortcomings of the subjective use of chromatographic analysis to determine the antigen concentration and achieving completely quantitative measurements.

4. Conclusions

In this study, we successfully combined the rapid test with an electrode detection chip that we designed. In the preparation of the NC membrane, the effects of porosity and film thickness on the flow rate of the specimen were studied, and the NC membrane phase was verified at a temperature of 30 °C and a relative humidity of 75–80%. The transformation of the NC membrane can achieve the best combination with the impedance electrode chip. On the other hand, we successfully transformed the conventional hCG qualitative detection into a quantitative detection using impedance measurement. Conventionally, the naked eye is used to observe the color development of the rapid screening reagent. When the concentration is lower than 50 mIU/mL, the chromaticity of the color gradually becomes lighter. However, by the impedance detection method in this study, the detected concentration can still be distinguished when the hCG concentration ranges from 6.25 to 50 mIU/mL. The coefficient of determination between the impedance and the hCG concentration reaches 0.9899. This shows that the impedance electrode chip developed in this study has been successfully combined with the NC membrane. In the future, it is expected to be combined with different detection items to provide a new immunoassay detection method for disease detection and medical analysis.

Acknowledgments

This research was supported by the National Science and Technology Council, Taiwan, under grant no. NSTC 112-2221-E-006-192. We express our deep gratitude for the help from those concerned.

References

1 R. C. Wong, and H. Y. Tse: Drugs of Abuse-Body Fluid Testing (HUMANA PRESS, 2005).
2 C. L. Wong, C. Y. Yong, H. K. Ong, K. L. Ho, and W. S. Tan: Front. Vet. Sci. **7** (2020). https://doi.org/10.3389/fvets.2020.00477
3 T. Watanabe, Y. Ohkubo, H. Matsuoka, H. Kimura, Y. Sakai, Y. Ohkaru, T. Tanaka, and Y. Kitaura: Clin. Biochem. **34** (2001) 257. https://doi.org/10.1016/S0009-9120(01)00200-4
4 A. J. Lapthorn, D. C. Harris, A. Littlejohn, J. W. Lustbader, R. E. Canfield, K. J. Machin, F. J. Morgan, and N. W. Isaacs: Nature **369** (1994) 455. https://doi.org/10.1038/369455a0
5 B. Faust, C. B. Billesbølle, C. M. Suomivuori, I. Singh, K. Zhang, N. Hoppe, A. F. M. Pinto, J. K. Diedrich, Y. Muftuoglu, M. W. Szkudlinski, A. Saghatelian, R. O. Dror, Y. Cheng, and A. Manglik: Nature **609** (2022) 846. https://doi.org/10.1038/s41586-022-05159-1
6 S. Birken, Y. Maydelman, M. A. Gawinowicz, A. Pound, Y. Liu, and A. S. Hartree: Endocrinology **137** (1996) 1402. https://doi.org/10.1210/endo.137.4.8625917
7 L. A. Cole: Reprod. Biol. Endocrinol. **7** (2009). https://doi.org/10.1186/1477-7827-7-8
8 L. Casarini, D. Santi, G. Brigante, and M. Simoni: Endocr. Rev. **39** (2018) 549. https://doi.org/10.1210/er.2018-00065
9 U. A. Kayisli, B. Selam, O. Guzeloglu-Kayisli, R. Demir, and A. Arici: J. Immunol. **171** (2003) 2305. https://doi.org/10.4049/jimmunol.171.5.2305
10 F. Shafiee, M. G. Aucoin, and A. Jahanian-Najafabadi: Front. Microbiol. **10** (2019). https://doi.org/10.3389/fmicb.2019.02340
11 P. Berger and C. Sturgeon: Trends Endocrinol. Metab. **25** (2014) 637. https://doi.org/10.1016/j.tem.2014.08.004
12 R. W. McNaught and J. T. France: J. Steroid Biochem. **13** (1980) 363. https://doi.org/10.1016/0022-4731(80)90017-5
13 M. Mulder: Basic Principles of Membrane Technology (Kluwer Academic Publishers, 1996).

14 T. Matsuura: Synthetic Membranes and Membrane Separation Processes (CRC Press, 1993).
15 Z. Sun, Z. S. Yang, Z. Y. Wang, and C. Y. Li: J. Membr. Sci. **563** (2018) 238. https://doi.org/10.1016/j.memsci.2018.06.003
16 Z. L. Cui, Y. M. Cheng, K. Xu, J. Yue, Y. Zhou, X. G. Li, Q. Wang, S. P. Sun, Y. Wang, X. Z. Wang, and Z. H Wang: Polymer **141** (2018) 46. https://doi.org/10.1016/j.polymer.2018.02.054
17 J. T. Jung, J. F. Kim, H. H. Wang, E. D. Nicolo, E. Drioli, and Y. M. Lee: J. Membr. Sci. **514** (2016) 250. https://doi.org/10.1016/j.memsci.2016.04.069
18 D. Zou, S. P. Nunes, I. F. J. Vankelecom, A. Figolid, and Y. M. Lee: Green Chem. **23** (2021) 9815. https://doi.org/10.1039/D1GC03318B
19 K. Xu, Y. C. Cai, N. T. Hassankiadeh, Y. M. Cheng, X. Li, X. O. Wang, Z. H. Wang, E. Drioli, and Z. L. Cui: Desalination **456** (2019) 13. https://doi.org/10.1016/j.desal.2019.01.004
20 D. M. Wang and J. Y. Lai: Curr. Opin. Chem. Eng. **2** (2013) 229. https://doi.org/10.1016/j.coche.2013.04.003
21 E. Rezabeigi, P. M. Wood-Adams, and R. A. L. Drew: Polymer **55** (2014) 6743. https://doi.org/10.1016/j.polymer.2014.10.063
22 S. H. Chen, R. M. Liou, Y. Y. Lin, C. L. Lai, and J. Y. Lai: Eur. Polym. J. **45** (2009) 1293. https://doi.org/10.1016/j.eurpolymj.2008.11.030
23 M. A. Hassen, G. Hamdy, R. M. Sabry, S. S. Ali, and F. A. Taher: Polym. Eng. Sci. **63** (2023) 509. https://doi.org/10.1002/pen.26225
24 A. Venault, M. R. B. Ballad, Y. T. Huang, Y. H. Liu, C. H. Kao, and Y. Chang: Chem. Eng. Sci. **142** (2016) 97. https://doi.org/10.1016/j.ces.2015.11.041
25 A. Venault, A. J. Jumao-as-Leyba, Z. R. Yang, S. Carretier, and Y. Chang: J. Taiwan Inst. Chem. Eng. **62** (2016) 297. https://doi.org/10.1016/j.jtice.2015.12.033
26 C. C. Lien, L. C. Yeh, A. Venault, S. C. Tsai, C. H. Hsu, G. V. Dizon, Y. T. Huang, A. Higuchi, and Y. Chang: J. Membr. Sci. **565** (2018) 119. https://doi.org/10.1016/j.memsci.2018.07.054
27 H. Y. Chang and A. Venault: J. Membr. Sci. **565** (2019) 178. https://doi.org/10.1016/j.memsci.2019.03.053
28 P. Zhang, S. Rajabzadeh, A. Venault, S. G. Wang, Q. Shen, Y. D. Jia, C. J. Fang, N. Kato, Y. Chang, and H. Matsuyama: J. Membr. Sci. **638** (2021) 119712. https://doi.org/10.1016/j.memsci.2021.119712
29 H. Caquineau, P. Menut, A. Deratani, and C. Dupuy: Polym. Eng. Sci. **43** (2003) 798. https://doi.org/10.1002/pen.10066
30 J. J. V. Aartsen, and C. A. Smolders: Eur. Polym. J. **6** (1970) 1105. https://doi.org/10.1016/0014-3057(70)90135-7
31 A. Dehban, A. Kargari, and F. Z. Ashtiani: J. Ind. Eng. Chem. **88** (2020) 292. https://doi.org/10.1016/j.jiec.2020.04.028
32 Z. H. Liu, J. Xiang, X. L. Hu, P. G. Cheng, L. Zhang, W. Du, S. B. Wang, and N. Tang: Chin. J. Chem. Eng. **34** (2021) 332. https://doi.org/10.1016/j.cjche.2020.11.038
33 S. Kiani, S. M. Mousavi, E. Saljoughi, and N. Shahtahmassebi: J. Non-Cryst. Solids **551** (2021) 120416. https://doi.org/10.1016/j.jnoncrysol.2020.120416
34 J. Y. Kim, Y. D. Kim, T. Kanamori, H. K. Lee, K. J. Baik, and S. C. Kim: J. Appl. Polym. Sci. **71** (1999) 431. https://doi.org/10.1002/(SICI)1097-4628(19990118)71:3<431::AID-APP9>3.0.CO;2-2
35 G. J. Chen, Y. Y. Yang, D. D Kang, Q. Q. Qin, J. B. Jin, H. J. Shao, and S. H. Qin: Sep. Purif. Technol. **258** (2021) 118043. https://doi.org/10.1016/j.seppur.2020.118043
36 C. Kahrs, M. Metze, C. Fricke, and J. Schwellenbach: J. Mol. Liq. **291** (2019) 111351. https://doi.org/10.1016/j.molliq.2019.111351
37 F. Farsaci, E. Tellone, A. Galtieri, and S. Ficarra: J. Mol. Liq. **291** (2019) 111319. https://doi.org/10.1016/j.molliq.2019.111319
38 N. Ismail, A. Venault, J. P. Mikkola, D. Bouyer, E. Drioli, and N. T. H. Kiadeh: J. Membr. Sci. **597** (2020) 117601. https://doi.org/10.1016/j.memsci.2019.117601
39 H. T. Lin, A. Venault, and Y. Chang: J. Membr. Sci. **614** (2020) 118543. https://doi.org/10.1016/j.memsci.2020.118543
40 R. Hintsche, M. Paeschke, U. Wollenberger, U. Schnakenberg, B. Wagner, and T. Lisec: Biosens. Bioelectron. **9** (1994) 697. https://doi.org/10.1016/0956-5663(94)80068-5
41 O. Niwa, M. Morita, and H. Tabei: Electroanalysis **3** (1991) 163. https://doi.org/10.1002/elan.1140030305
42 A. J. Gross, and F. Marken: Electrochem. Commun. **46** (2014) 120. https://doi.org/10.1016/j.elecom.2014.06.025
43 P. S. Pakchin, S. A. Nakhjavani, R. Saber, H. Ghanbari, and Y. Omidi: Trends Anal. Chem. **92** (2017) 32. https://doi.org/10.1016/j.trac.2017.04.010
44 S. Campuzano, P. Yánez-Sedeño, and J. M. Pingarrón: Trends Anal. Chem. **86** (2017) 14. https://doi.org/10.1016/j.trac.2016.10.002
45 N. Alizadeh, A. Salimi, and R. Hallaj: J. Electroanal. Chem. **811** (2018) 8. https://doi.org/10.1016/j.jelechem.2017.12.080

About the Authors

Wei-Chien Weng received his M.S. degree in engineering science from National Cheng Kung University of Education in 2017. His main research interests include microstructure design, biomedical applications, and biomedical equipment development. He is currently a doctoral student in the Department of Engineering Science at National Cheng Kung University, Tainan, Taiwan. (lu4a04@gmail.com / n98104028@gs.ncku.edu.tw)

Yu-Lin Wu received his M.S. degree in computer science and information engineering from National Changhua University of Education in 2017. He is currently a doctoral student in the Department of Engineering Science at National Cheng Kung University, Tainan, Taiwan. (n98091039@gs.ncku.edu.tw)

Hsin-Yu Chen received her M.S. degree in engineering science from National Cheng Kung University of Education in 2019. Her main research interests include microstructure design, biomedical applications, and semiconductor processes. She is an engineer at TSMC, Taiwan. (nckuyuclin@gmail.com)

Yu-Cheng Lin received his Ph.D. degree in electrical engineering from the University of Illinois at Chicago in 1996. He is a Distinguished Professor in the Department of Engineering Science at National Cheng Kung University, Tainan, Taiwan. His main research interests include bio-MEMS, microfluidic systems, and nanotechnology in biomedical applications. He is currently an associate editor of IEEE Sensors Journal and an editorial advisory board member of Sensors and Actuators A: Physical. He was the Vice President of Conferences of IEEE Sensors Council for 2014–2017. He was elected as a Fellow of the Royal Society of Chemistry in 2008, a Fellow of the International Society for Optics and Photonics (SPIE) in 2012, and a Fellow of the Institution of Engineering and Technology (IET) in 2013. (yuclin@mail.ncku.edu.tw)